The 14th World Conference on Earthquake Engineering
October 12-17, 2008, Beijing, China

DIFFRACTION OF SEISMIC WAVES FROM 3-D CANYONS AND ALLUVIAL BASINS MODELED USING THE FAST MULTIPOLE-ACCELERATED BEM

S. CHAILLAT[1], M. BONNET[2] and J.F. SEMBLAT[3]

[1] PhD Student, Laboratoire de Mécanique des Solides, École Polytechnique, France,
& Laboratoire Central des Ponts et Chaussées, Paris, France
Email: chaillat@lms.polytechnique.fr
[2] Senior scientist, Laboratoire de Mécanique des Solides, École Polytechnique, France,
[3] Senior scientist, Laboratoire Central des Ponts et Chaussées, Paris, France

ABSTRACT:

The analysis of seismic wave propagation and amplification in complex geological structures raises the need for efficient and accurate numerical methods. The solution of the elastodynamic equations using boundary element methods (BEMs) gives rise to fully-populated matrix equations. Earlier investigations on the elastodynamic equations have established that the Fast Multipole (FM) method reduces the complexity of a BEM solution to $N \log N$ per GMRES iteration. The present Article addresses the extension of the FM-BEM strategy to 3D multi-domain elastodynamics in the frequency domain. Using this FM-accelerated BEM it is now possible to study the propagation of seismic waves in 3-D alluvial basins at a much lower cost than with standard BEM. Validations are performed for canonical basins and comparisons to previous works are proposed. It shows the efficiency and accuracy of the fast BEM formulation proposed.

KEYWORDS: site effects, boundary element method, seismic wave amplification, Fast Multipole Method.

1 INTRODUCTION

Seismic site effects are a major concern for earthquake engineering because very large local amplifications of seismic motions may occur. Such phenomena can strengthen the surface ground motion and increase the consequences on structures and buildings. To analyze site effects, it is possible to consider modal approaches or directly investigate wave propagation phenomena. The importance of 2D and 3D simulations is well recognized throughout the literature. A lot of studies have been devoted to the 2D case. The 3D case is currently a very attractive field of research because of the increase of the speed and capabilities of computers. To compute seismic wave propagation in alluvial basins, various numerical methods have been proposed: the series expansions, the multipolar expansions of wave functions, the finite element method, the finite differences, the spectral elements method, the boundary element method [BEM, see e.g. Bonnet, 1999, Dangla et al., 2005]. The main advantage of the latter is that only

the domain boundaries (and possibly interfaces) are discretized, leading to a reduction of the number of degrees of freedom (DOFs). However, the standard BEM leads to fully-populated, non-symmetric matrices. This entails high computational costs, both in CPU time ($O(N^2)$ per iteration using an iterative solver such as GMRES) and memory requirements ($O(N^2)$), where N denotes the number of DOFs of the BEM model.

In other research areas where the BEM is used (electromagnetism, acoustics,...), considerable speedup of solution time and decrease of memory requirements has been achieved, over the last decade, through the development of the Fast Multipole Method (FMM) [Nishimura, 2002]. This method is known to reduce the CPU time to $O(N \log_2 N)$ per iteration. So far, very few studies have been devoted to the FMM in elastodynamics (see, however, [Fujiwara, 2000] for the frequency-domain case and [Takahashi et al., 2003] for the time-domain case). The present article improves on the methodology of [Fujiwara, 2000] by incorporating recent advances of FMM implementations for Maxwell equations (e.g. [Darve, 2000]), which allow to run BEM models of much larger size.This paper is organized as follows. First, the main features of the elastodynamic FMM-BEM formulation are concisely presented. Then, numerical efficiency and accuracy are assessed on numerical results obtained for problems with well-known solutions. Finally, the efficiency of the present FMM-BEM is demonstrated on seismology-oriented examples.

2 STANDARD AND FAST MULTIPOLE ACCELERATED BOUNDARY ELEMENT METHOD

2.1 *Single-region boundary element method*

Let Ω denote a region of space occupied by an isotropic elastic solid characterized by μ (shear modulus), ν (Poisson's ratio) and ρ (mass density). Assuming a time-harmonic motion with circular frequency ω, the displacement can be written:

$$\boldsymbol{u}(\boldsymbol{x}, t) = \tilde{\boldsymbol{u}}(\boldsymbol{x}, \omega) e^{i\omega t} \tag{2.1}$$

In the following, the factor $e^{i\omega t}$ is systematically omitted and the notation $\boldsymbol{u}$ is used instead of $\tilde{\boldsymbol{u}}$. Assuming the absence of body forces, the displacement $\boldsymbol{u}$ is given at an interior point $\boldsymbol{x} \in \Omega$ by the well-known representation formula:

$$u_k(\boldsymbol{x}) = \int_{\partial\Omega} [t_i(\boldsymbol{y}) U_i^k(\boldsymbol{x}, \boldsymbol{y}; \omega) - u_i(\boldsymbol{y}) T_i^k(\boldsymbol{x}, \boldsymbol{y}; \omega)] \, \mathrm{d}S_y \tag{2.2}$$

where $\boldsymbol{t}$ is the traction vector on the boundary $\partial\Omega$, and $U_i^k(\boldsymbol{x}, \boldsymbol{y}; \omega)$ and $T_i^k(\boldsymbol{x}, \boldsymbol{y}; \omega)$ denote the i-th components of the elastodynamic fundamental solution, i.e. of the displacement and traction, respectively, generated at $\boldsymbol{y} \in \mathbb{R}^3$

by a unit point force applied at $\boldsymbol{x} \in \mathbb{R}^3$ along the direction k [Eringen and Suhubi, 1975]:

$$\begin{aligned} U_i^k(\boldsymbol{x},\boldsymbol{y};\omega) = &\quad \frac{1}{4\pi k_S^2 \mu}\Big((\delta_{qs}\delta_{ik}-\delta_{qk}\delta_{is})\frac{\partial}{\partial x_q}\frac{\partial}{\partial y_s}G(|\boldsymbol{y}-\boldsymbol{x}|;k_S)+\frac{\partial}{\partial x_i}\frac{\partial}{\partial y_k}G(|\boldsymbol{y}-\boldsymbol{x}|;k_P)\Big), \\ T_i^k(\boldsymbol{x},\boldsymbol{y};\omega) = &\quad \mu\Big[\frac{2\nu}{1-2\nu}\delta_{ij}\delta_{k\ell}+\delta_{ik}\delta_{j\ell}+\delta_{jk}\delta_{i\ell}\Big]\frac{\partial}{\partial y_\ell}U_h^k(\boldsymbol{x},\boldsymbol{y};\omega)n_j(\boldsymbol{y}), \\ &\quad k_S^2=\frac{\rho\omega^2}{\mu},\quad k_P^2=\frac{1-2\nu}{2(1-\nu)}k_S^2 \end{aligned} \tag{2.3}$$

in which $G(r;k)$, defined by

$$G(r;k)=\frac{\exp(ikr)}{4\pi r} \tag{2.4}$$

is the free-space Green's function for the Helmholtz equation with wavenumber k_α corresponding to either P or S elastic waves, and $\boldsymbol{n}(\boldsymbol{y})$ is the unit normal to $\partial\Omega$ directed outwards of Ω.

When $\boldsymbol{x} \in \partial\Omega$, a singularity occurs at $\boldsymbol{y}=\boldsymbol{x}$. With the help of a well-documented limiting process, the integral representation (2.2) yields the integral equation, for $\boldsymbol{x} \in \partial\Omega$:

$$c_{ik}(\boldsymbol{x})u_i(\boldsymbol{x}) = \int_{\partial\Omega} t_i(\boldsymbol{y})U_i^k(\boldsymbol{x},\boldsymbol{y};\omega)\mathrm{d}S_y - (\text{P.V.})\int_{\partial\Omega} u_i(\boldsymbol{y})T_i^k(\boldsymbol{x},\boldsymbol{y};\omega)\mathrm{d}S_y \tag{2.5}$$

where (P.V.) indicates a Cauchy principal value (CPV) singular integral and the *free-term* $c_{ik}(\boldsymbol{x})$ is equal to $0.5\delta_{ik}$ in the usual case where $\partial\Omega$ is smooth at $\boldsymbol{x}$. Equation (2.5) may be recast into alternative, equivalent regularized forms which are free of CPV integrals [Dangla et al., 2005].

The numerical solution of boundary integral equation (2.5) is based on a boundary element (BE) discretization of the surface $\partial\Omega$ and boundary traces (u,t), leading to the system:

$$[H]\{u\}+[G]\{t\}=0, \tag{2.6}$$

where $[H]$ and $[G]$ are fully populated, nonsymmetric, matrices and vectors $\{u\}$, $\{t\}$ gather the displacement and traction degrees of freedom (DOFs). In this work, linear three-noded triangular boundary elements are used, together with a piecewise-linear continuous (i.e. isoparametric) interpolation for the displacements and a piecewise-constant interpolation of tractions. Upon introduction of boundary conditions, the matrix equation (2.6) is recast in the form:

$$[K]\{v\}=\{f\}, \tag{2.7}$$

where the N-vector $\{v\}$ collects the sought degrees of freedom (DOFs), while the $N \times N$ matrix of influence coefficients $[K]$ contains the columns of $[H]$ and $[G]$ associated with the unknown components.

BEM matrix equations such as (2.7) are here solved iteratively using the GMRES algorithm. The influence matrix $[K]$ is fully-populated. With reference to (2.7), each GMRES iteration requires one evaluation of $[K]\{u\}$ for given $\{u\}$, a task requiring a computing time of order $O(N^2)$ if either $[K]$ is stored or $[K]\{u\}$ is evaluated by means of standard BEM numerical integration procedures. This $O(N^2)$ complexity, unacceptable for large BEM models, can be lowered by resorting to fast BEM solutions techniques such as the Fast Multipole Method (FMM).

2.2 *Fast Multipole Method: principle*

The goal of the FMM is to speed up the matrix-vector product computation required for each iteration of the iterative solver applied to the BEM-discretized equations. Moreover, the governing BEM matrix is never explicitly formed, which leads to a storage requirement well below the $O(N^2)$ memory required for holding it. Substantial savings in both CPU time and memory are thus achieved.

In general terms, the FMM exploits a reformulation of the fundamental solutions in terms of products of functions of $\boldsymbol{x}$ and of $\boldsymbol{y}$, so that (in contrast with the traditional BEM) integrations with respect to $\boldsymbol{y}$ can be reused when the collocation point $\boldsymbol{x}$ is changed. On decomposing the position vector $\boldsymbol{r} = \boldsymbol{y}-\boldsymbol{x}$ into $\boldsymbol{r} = (\boldsymbol{y} - \boldsymbol{y_0})+\boldsymbol{r_0}-(\boldsymbol{x} - \boldsymbol{x_0})$, where $\boldsymbol{x_0}$ and $\boldsymbol{y_0}$ are two poles and $\boldsymbol{r_0} = \boldsymbol{y_0} - \boldsymbol{x_0}$ and invoking the Gegenbauer addition theorem, the Helmholtz Green's function is written as [Darve, 2000]:

$$G(|\boldsymbol{r}|, k) = \lim_{L\to+\infty} \int_{\hat{\boldsymbol{s}}\in S} e^{ik\hat{\boldsymbol{s}}.(\boldsymbol{y}-\boldsymbol{y_0})} \mathcal{G}_L(\hat{\boldsymbol{s}}; \boldsymbol{r_0}; k) e^{-ik\hat{\boldsymbol{s}}.(\boldsymbol{x}-\boldsymbol{x_0})} d\hat{\boldsymbol{s}}, \tag{2.8}$$

where S is the unit sphere of $\mathbb{R}^3$ and the *transfer function* $\mathcal{G}_L(\hat{\boldsymbol{s}}; \boldsymbol{r_0}; k)$ is defined in terms of the Legendre polynomials P_p and the spherical Hankel functions of the first kind $h_p^{(1)}$ by:

$$\mathcal{G}_L(\hat{\boldsymbol{s}}; \boldsymbol{r_0}; k) = \frac{ik}{16\pi^2} \sum_{0\le p\le L} (2p+1) i^p h_p^{(1)}(k|\boldsymbol{r_0}|) P_p\big(cos(\hat{\boldsymbol{s}}, \boldsymbol{r_0})\big) \tag{2.9}$$

Then, the elastodynamic fundamental solution (2.3) is easily seen to admit representations of the form (2.8) with $\mathcal{G}_L$ replaced with suitably-defined (tensorial) transfer functions [Chaillat et al., 2008].

A 3D cubic grid of linear spacing d embedding the whole boundary $\partial\Omega$ is then introduced. The FMM basically consists of using decomposition (2.8), with the poles $\boldsymbol{x_0}$ and $\boldsymbol{y_0}$ being chosen as the cell centers, whenever $\boldsymbol{x}$ and $\boldsymbol{y}$ belong to *non-adjacent* cubic cells. The treatment of such "FM" contributions exploits the multipole expansions of the fundamental solutions (2.3), truncated at a finite L and in a manner suggested by their multiplicative form. When $\boldsymbol{x}$ and $\boldsymbol{y}$ belong to adjacent cells, traditional BEM evaluation methods based on expressions (2.3) and (2.4) are used. To improve further the computational efficiency of the FM-BEM, standard (i.e. non-FMM) calculations must be confined to the smallest possible spatial regions while retaining the advantage of clustering the computation of influence terms into non-adjacent large groups whenever possible. This idea is carried out by subdividing cubic cells into eight smaller cubic cells. New pairs of non-adjacent smaller cells, to which multipole expansions are applicable, are thus obtained from the subdivision of pairs of adjacent cells. This is the essence of the multi-level FMM, whose theoretical complexity is $O(N \log N)$ per GMRES iteration both for CPU time and memory (see [Chaillat et al., 2008] for further details on the method and its implementation for single-domain elastodynamic problems). This formulation will now be generalized to seismic wave propagation in alluvial basins.

2.3 *Boundary Element-Boundary Element coupling strategy*

In the case of multi-domain problems, the boundary of each subregion Ω_j generally contains boundary elements and nodes, located on Γ_j, that belong only to Ω_j, and interfacial boundary elements and nodes belonging to Γ_{ij}

for some $i \neq j$. The governing boundary integral equation can then be written for each zone. A system of matrix equations for each zone is obtained. The matrix relations written for each of the individual zones can be assembled for use in an overall analysis by considering the conditions of displacement compatibility and equilibrium of the traction components at all interfaces.

To build the discrete problem, piecewise-linear interpolation of displacements, based on three-noded triangular boundary elements is used. Because of the equilibrium of the traction, piecewise-constant interpolation of tractions based on boundary elements are used. In the case of multi-domain problems, a boundary integral equation is formulated for each subregion Ω_i (with material properties assumed homogeneous in each Ω_i). The matrix-vector products arising in each of these integral equations can be evaluated using the FM-BEM procedure for homogeneous media presented in the previous section. Each subregion is thus treated separately, with the help of a separate octree.

3 Propagation and amplification of seismic waves in alluvial basins.

In [Chaillat et al., 2008], the single-domain elastodynamic FMM has been checked for the case of the scattering by an irregular surface of a plane P-wave with vertical incidence and normalized frequency $k_P a/\pi = 0.25$ (with $\nu = 0.25$) against the results of [Sánchez-Sesma, 1983], and then applied to the same configuration with a higher frequency ($k_P a/\pi = 5$). In this section, the present implementation is checked in the case of the propagation of seismic waves in alluvial basins.

3.1 *Diffraction of an incident plane P-wave by a single-layered semi-spherical basin*

This first example is concerned with the diffraction by a semi-spherical alluvial basin (i.e. soft elastic inclusion) of a plane P-wave of unit amplitude traveling vertically in an elastic homogeneous irregular half-space (Fig. 3.1). Such a configuration may lead to a strong amplification of the seismic motion in soft alluvial deposits.

We investigate the motion at the surface of the alluvial basin Ω_2, for the following values of the material parameters: $\mu^{(2)} = 0.3\mu^{(1)}$, $\rho^{(2)} = 0.6\rho^{(1)}$, $\nu^{(1)} = 0.25$ and $\nu^{(2)} = 0.3$. The normalized frequency is defined by $k_P^{(1)} a/\pi$, i.e. in terms of the properties of the elastic semi-infinite medium Ω_1. The size of the discretized free surface is chosen equal to $D = 5a$ (as in [Sánchez-Sesma, 1983]).

Table 3.1: Diffraction of an incident plane P-wave by a semi-spherical alluvial basin: data and computational results

$k_P^{(1)} a/\pi$	N	$\bar{l}_1; \bar{l}_2$	CPU (s) / iter	nb iter.
0.5	17,502	3, 3	8	39
2	190,299	5, 4	79	627

The surface displacements computed with the present multi-domain FMM are presented, along with corresponding

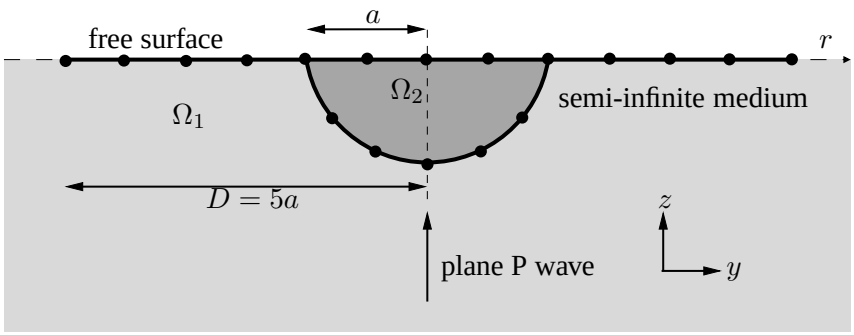

Figure 3.1: Diffraction of an incident plane P-wave by a semi-spherical alluvial basin: notations

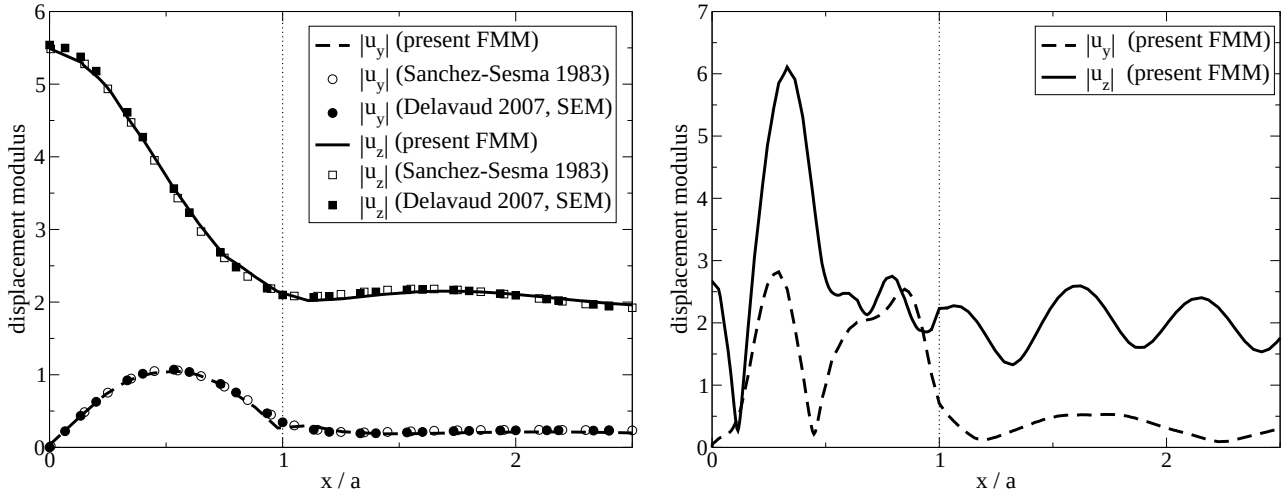

Figure 3.2: Diffraction of an incident plane P-wave by a semi-spherical alluvial basin (left: $k_P^{(1)} a/\pi = 0.5$, right: $k_P^{(1)} a/\pi = 2$)

results from [Sánchez-Sesma, 1983] and [Delavaud, 2007], for $k_P^{(1)} a/\pi = 0.5$ (Fig. 3.2, left). The results are seen to be in good agreement.

Additionally, the FMM allowed to perform computations for higher frequency $k_P^{(1)} a/\pi = 2$ (Fig. 3.2, right). In Table 3.1, the number of DOFs and the leaf level $\bar{\ell}_i$ in each subdomain Ω_i are given for the meshes used, together with the CPU time per iteration and iteration counts recorded. The last example indicates that the iteration count significantly impacts the computational efficiency for problem sizes for which the CPU time per iteration and the memory requirements are still moderate. An efficient preconditioning strategy is needed and will be addressed in future investigations.

3.2 *Diffraction of an incident plane P-wave by a two-layered semi-spherical basin*

The examples presented in section 3.1 were limited to a single-layered basin, whereas the present implementation is in fact applicable to more general configurations featuring n subregions ($n \geq 1$). To demonstrate this capability, the diffraction of an incident plane P-wave by a heterogeneous semi-spherical basin is now considered for an alluvial deposit composed of two layers (Fig. 3.3). The two layers Ω_2 and Ω_3 are made of different materials, with mechanical properties defined so that the velocity contrast between Ω_1, Ω_2 and between Ω_2, Ω_3 are the same:

$$\frac{\rho^{(2)}}{\rho^{(1)}} = \frac{\rho^{(3)}}{\rho^{(2)}} = 0.6; \qquad \frac{\mu^{(2)}}{\mu^{(1)}} = \frac{\mu^{(3)}}{\mu^{(2)}} = 0.3; \qquad \nu^{(1)} = 0.25; \qquad \nu^{(2)} = \nu^{(3)} = 0.30 \tag{3.1}$$

The thickness $h^{(2)}$ and $h^{(3)}$ of the layers Ω_2 and Ω_3 are adapted to the wavelengths:

$$\frac{h^{(2)}}{\lambda_s^{(2)}} = \frac{h^{(3)}}{\lambda_s^{(3)}} \quad \Rightarrow \quad h^{(2)} = \frac{\sqrt{2}a}{(1+\sqrt{2})}; \quad h^{(3)} = \frac{a}{(1+\sqrt{2})} \tag{3.2}$$

The mesh features $N = 91,893$ DOFs. The normalized frequency is $k_p^{(1)} a/\pi = 1$. The computation takes 248 iter., 48 s/iter ($\bar{\ell}_1 = 4$, $\bar{\ell}_2 = 3$, $\bar{\ell}_3 = 3$).

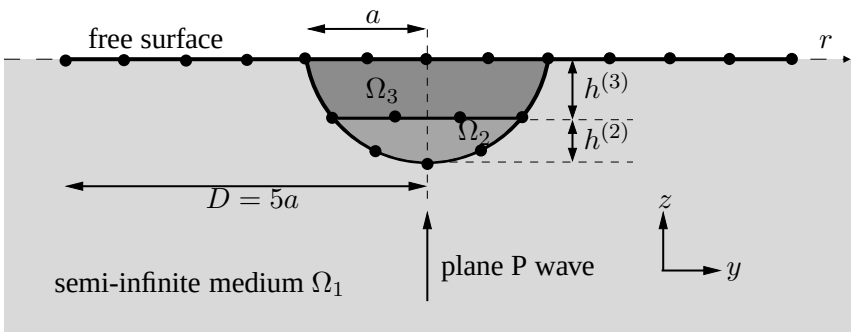

Figure 3.3: Diffraction of an incident plane P-wave by a two-layered semi-spherical basin: notation.

In Figure 3.4, the results of the computation for the two-layered semi-spherical basin are compared to those for a one-layered basin. The introduction of the layer Ω_3 leads to stronger amplification, with shorter wavelengths, in the basin.

4 Conclusion

In this article, a multi-level fast multipole multi-domain formulation has been proposed, based on previous works on single-region FMM [Chaillat et al., 2008]. Comparisons with the analytical or previously published numerical results show the efficiency and accuracy of the present implementation. The studies of seismic wave propagation

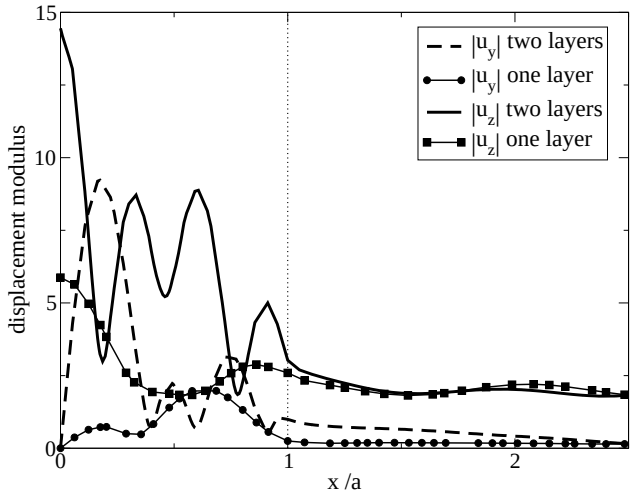

Figure 3.4: Diffraction of an incident plane P-wave by a two-layered semi-spherical basin ($k_p^{(1)} a/\pi = 1$).

in canonical basins for higher frequencies than in previously published results show the numerical efficiency of the method and suggest that it is suitable to deal with realistic seismological applications. The transient response of 3-D basins has also been investigated to illustrate the large domain of application of the method. Moreover, because the hypothesis of a linear elastic soil is often not sufficient, the extension of the present work to linear viscoelasticty is under way.

REFERENCES

Bonnet, M. (1999). Boundary Integral Equation Method for Solids and Fluids, Wiley.

Chaillat, S., Bonnet, M. and Semblat J.F. (2008). A multi-level fast multipole BEM for 3-D elastodynamics in the frequency domain. *Comp. Meth. Appl. Mech. Engng.*, **to appear**.

Dangla, P., Semblat, J.F., Xiao, H. and Delépine, N. (2005). A simple and efficient regularization method for 3D BEM: application to frequency-domain elastodynamics. *Bull. Seism. Soc. Am.*, **95:5,**1916-1927.

Darve, E. (2000). The fast multipole method: Numerical implementation. *J. Comp. Phys.*, **160:1,**195-240.

Delavaud, E. (2007). Simulation numérique de la propagation d'ondes en milieu géologique complexe : application à l'évaluation de le réponse sismique du bassin de Caracas (Venezuela). *PhD thesis, IPG, Paris.*

Eringen, A.C. and Suhubi, E.S. (1975). Elastodynamics, volume II-linear theory. Academic Press.

Fujiwara, H. (2000). The fast multipole method for solving integral equations of three-dimensional topography and basin problems. *Geophysical Journal International*, **140:1,**198-210.

Nishimura, N. (2002). Fast multipole accelerated boundary integral equation methods. *Appl. Mech. Rev.*, **55:4,**299-324.

Sánchez-Sesma, F.J. (1983). Diffraction of elastic waves by 3D surface irregularities. *Bull. Seism. Soc. Am.*, **73:6,**1621-1636.

Takahashi, T., Nishimura, N. and Kobayashi, S.(2003). A fast BIEM for three-dimensional elastodynamics in time domain. *Engineering Analysis with Boundary Elements*, **27:2,**491-506.